ACS Catalysis

Research Article

pubs.acs.org/acscatalysis

Role of Lewis and Brønsted Acid Sites in the Dehydration of Glycerol over Niobia

Guo Shiou Foo, Daniel Wei, David S. Sholl, and Carsten Sievers*

School of Chemical & Biomolecular Engineering, Georgia Institute of Technology, 311 Ferst Drive NW, Atlanta, Georgia 30332, United States

Supporting Information

ABSTRACT: The role of Lewis and Brønsted sites in the dehydration of glycerol on niobium oxide and Na^+-exchanged niobium oxide is investigated using FTIR spectroscopy supported by DFT calculations. Glycerol is impregnated on the catalysts at room temperature using an *ex-situ* method. Under high vacuum conditions, glycerol forms a stable multidentate alkoxy species through its primary hydroxyl groups with the Lewis sites. When coordinated this way, the primary C−O bonds are polarized, favoring dehydration in this position to form hydroxyacetone. In contrast, dehydration of the secondary alcohol group is kinetically favored over Brønsted acid sites in the absence of steric constraints. The primary product of this reaction, 1,3-propenediol, is further dehydrated to acrolein. When more than a monolayer of glycerol is impregnated on niobia, monoaromatic compounds are also formed on the surface upon heating.

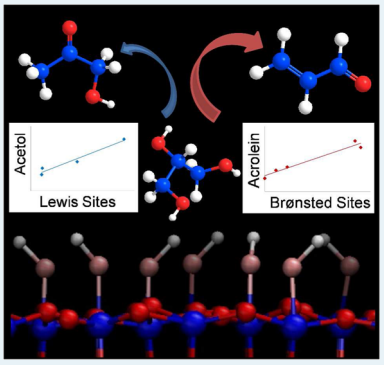

KEYWORDS: *glycerol, niobium oxide, Lewis acid, Brønsted acid, dehydration*

1. INTRODUCTION

Glycerol is a major byproduct from the transesterification of vegetable oils and fats to produce biodiesel. Biodiesel production in U.S. has increased significantly from 500 000 gallons in 1999 to 967 million gallons in 2011.[1] To ensure that this industry remains economically viable, it is crucial to convert glycerol to value-added chemicals by catalytic processes such as dehydration, reforming, oxidation, etherification, esterification, and hydrogenolysis.[2] Acrolein is an important product from the dehydration of glycerol. It is currently produced by the selective oxidation of propylene.[3] Besides being used in the synthesis of acrylic acid,[4] acrolein is also needed in the synthesis of DL-methionine, which is an essential amino acid.[5]

Many studies have been performed on the dehydration of glycerol, but controlling the selectivity of this reaction remains a challenge.[6] Early work focused on the reaction in the aqueous phase under near- or at supercritical conditions using homogeneous catalysts.[7,8] However, due to the estimated high cost of reaction vessel and separation issues, the dehydration of glycerol in the vapor phase over heterogeneous catalysts is preferred. Typical gas phase reactions are carried out in the temperature range of 250−350 °C using aqueous glycerol as a feedstock.[5] A number of solid acid catalysts have been reported including zeolites, heteropoly acids, niobia, and alumina.[2,9−17] The selectivity of acrolein has been correlated with low Hammett acidity.[10,18] Low selectivity of acrolein has been reported over Lewis acids.[10] However, there is only limited insight regarding the reason for the differences in the performance of different acid sites. Therefore, it is crucial to gain such understanding and to control the type, strength, and concentration of acid sites on solid acid catalysts for optimized performance for the production of acrolein.

Nimlos et al. investigated the dehydration of neutral and protonated glycerol using quantum mechanical calculations[19] and found that protonation will significantly lower dehydration temperatures. Laino et al. used metadynamics simulations to study the dehydration of neutral glycerol in the gas phase and suggested glycerol decomposition via glycidol formation.[20] These studies, however, did not consider the influence of catalysts.

There are a few reports on surface interactions and dehydration reactions of glycerol on different solids, in which FTIR spectroscopy was used as the main technique.[21−24] Glycerol was adsorbed on H-MFI and silica−alumina by heating up the vacuum line to 353 K, but the amount of glycerol deposited could not be estimated.[21,22] Moreover, the dehydration reaction could have occurred at the deposition temperature in the presence of a catalyst as a peak due to the carbonyl stretching mode (1656 cm^{-1}) was observed without further heating. To solve this problem, Copeland et al. devised an *ex-situ* method of impregnating a controlled amount of glycerol on γ-Al_2O_3.[23] This method can be performed at room temperature, thus preventing glycerol from reacting prematurely.

In this study, we report the role of Lewis and Brønsted acid sites in the dehydration of glycerol using transmission FTIR spectroscopy with the aid of density functional theory (DFT)

Received: May 9, 2014
Revised: July 6, 2014
Published: August 11, 2014

   dx.doi.org/10.1021/cs5006376 | ACS Catal. 2014, 4, 3180−3192

calculations. The *ex-situ* impregnation method is used here to contact glycerol with niobium oxide, which is water-tolerant and possesses relatively strong Lewis and Brønsted acid sites.[25−29] Most importantly, the Brønsted sites can be blocked by Na^+,[29] which allows elucidating the role of different acid sites.

2. EXPERIMENTAL SECTION

2.1. Materials. Glycerol (99%), acrolein (90%), hydroxyacetone (90%), NaCl (>99%), NaOH (>98%), and pyridine (>99%) were purchased from Sigma-Aldrich and were used as received. Niobic acid (HY-340) was provided by CBMM (Brazil). Niobium oxide was obtained by calcining niobic acid under flowing air (200 mL/min) at a ramp rate of 10 K/min for 4 h at selected temperatures (350 °C, 400 °C, 500 °C, 600 °C, 700 °C). The samples are named as NBX, where X is the calcination temperature.

2.2. Synthesis of Na^+/NB500. The synthesis procedure was modified from a report in the literature.[29] Na^+ exchange of NB500 was performed by stirring 500 mg of NB500 in 200 mL of 1 M NaCl solution maintained at 60 °C and pH = 11.0−11.4. The pH was adjusted periodically by adding 0.05 M NaOH solution. After 52 h when the pH stops decreasing, the sample was collected and washed repeatedly with distilled water until Cl^- ions were no longer detected. The sample was then dried in an oven at 100 °C for 12 h.

2.3. Catalyst Characterization. Nitrogen sorption measurements at 77 K were performed with a Micromeritics ASAP 2020 physisorption analyzer. Prior to the measurement, the samples were degassed under a vacuum at 150 °C for 5 h. Surface areas were calculated using the BET method,[30] and pore volumes were calculated on the basis of the adsorption branch of the isotherm using the BJH method.[31] X-ray diffraction (XRD) measurements were performed with a Philips X'pert diffractometer equipped with an X'celerator module using Cu Kα radiation. Diffractograms were collected at incident angles from 2θ = 5 to 70° with a step size of 0.0167°. Thermal gravimetric analysis (TGA) of niobic acid was performed using a TA Instruments SDT Q600 thermal analyzer. For each experiment, 2.0 mg of niobic acid was loaded into an aluminum pan and heated in flowing air (50 mL/min) from room temperature to 800 °C at a rate of 10 K/min. Raman spectra were collected on a Bruker FRA-106. A total of 1028 scans were collected with a resolution of 2−4 cm^{-1}. A powder sample was placed in a small hemispherical sample holder. Pyridine adsorption followed by IR spectroscopy was obtained using a Nicolet 8700 FTIR spectrometer with a MCT/A detector. For each spectrum, 64 scans were recorded at a resolution of 4 cm^{-1}. Each sample was pressed into a self-supported wafer and loaded into a transmission vacuum chamber. The sample was activated at 350 °C for 1 h under a high vacuum and cooled down to room temperature. A background spectrum was collected. Pyridine was then introduced into the chamber at 0.1 mbar for 30 min followed by evacuation for 1 h, and a spectrum was collected. For the evaluation of acid strength, the sample was heated at 150, 250, and 350 °C for 1 h to desorb pyridine on weak acid sites, and spectra were collected at room temperature. After each experiment, the wafer was cut using a circular stamp with a diameter of 6.35 mm and weighed to determine the density. The concentration of Lewis and Brønsted acid sites was determined from the integral of the peaks at 1445 and 1540 cm^{-1}, respectively, and the density of the wafer. The molar extinction coefficients used were reported by Nakajima et al.[29]

2.4. FTIR Spectroscopy. Niobium oxide was impregnated with glycerol via an *ex-situ* method.[23] For each niobium oxide sample, 250 mg was weighed and mixed with 10 mL of dilute aqueous glycerol solution. The concentration of the solution was chosen such that there is a deposition of the desired amount on the niobium oxide to achieve the desired loading, which typically ranges from 2 to 3 wt %. After 24 h, the slurry was dried using a Schlenk line at room temperature for 8 h to obtain a dry glycerol impregnated sample. To prepare appropriate samples as subtrahends for difference spectra, each niobium oxide sample was mixed with 10 mL of distilled water for 24 h and dried using the same method. Each impregnated sample was pressed into a self-supported wafer and loaded into a transmission vacuum chamber.

A spectrum was collected under room temperature and pressure (RTP) using an empty cell background with the same conditions. The cell was subjected to high vacuum conditions ($<10^{-6}$ mbar), and a spectrum was collected again using an empty cell background under the same conditions (RTHV). The wafer was then heated at 100 °C, 150 °C, 200 °C, 250 °C, 300 °C, and 350 °C for 1 h, and a spectrum was collected at each temperature. For experiments in the presence of water vapor, the cell was dosed with 1 mbar of water vapor for 1 h after evacuation, followed by the same heating procedure. After each experiment, the wafer was cut using a circular stamp with a diameter of 6.35 mm and weighed to determine the density.

A different procedure was used to adsorb acrolein or hydroxyacetone on NB500. The pure catalyst was pressed into a self-supported wafer and loaded into a transmission vacuum chamber. The sample was activated at 350 °C for 1 h under high vacuum conditions and was cooled down to room temperature. A background spectrum was collected. Acrolein or hydroxyacetone was introduced into the chamber as vapors at 0.1 mbar through a leak valve for 15 min. Afterward, the cell was evacuated for 1 h, and a spectrum was collected. The sample was then heated at 150, 250, and 350 °C for 1 h, and a spectrum was collected at each temperature. The spectra of liquid acrolein and hydroxyacetone were collected using an ATR accessory at room temperature.

All spectra were collected using a Nicolet 8700 FTIR spectrometer with a MCT/A detector. For each spectrum, 64 scans were recorded at a resolution of 4 cm^{-1}. Thermo Fischer Scientific Inc. Grams 9.1 software was used to process the difference spectra. The spectrum of each reactant-free niobium oxide was subtracted from the respective sample. The subtrahend spectrum was collected at room temperature after heating at 350 °C for 1 h. All spectra were normalized by its wafer density prior to subtraction.

2.5. DFT Calculations. Periodic density functional theory (DFT) calculations were performed with the Vienna *ab initio* simulation package (VASP).[32−35] Electron−electron exchange and correlation was described with the PW-91 GGA functional, and the electron−core interaction was described with the projector augmented wave (PAW) method.[36−39] The cutoff energy for the plane wave basis set was fixed at 400 eV. Structural relaxation was performed through a conjugate-gradient algorithm and was considered to be converged when the forces on each unconstrained atom were <0.03 eV/Å. Due to the size of the supercell, which contained over 300 atoms, reciprocal space was only sampled at the Γ point. The surface slab was modeled with the T-phase of Nb_2O_5.[40] The crystalline

dx.doi.org/10.1021/cs5006376 | ACS Catal. 2014, 4, 3180−3192

structure was obtained through the Inorganic Crystal Structure Database,[41] and preliminary calculations had shown that the Nb terminated (100) surface had the lowest surface energy. Additionally, preliminary calculations had shown the inclusion of Nb atoms in the interstitial sites did not significantly impact the surface property; thus, interstitial Nb atoms were excluded in the calculations. The surface slab had a thickness of 7 Å with the bottom-most 4 Å immobilized. After relaxation of the surface, the entire surface slab was immobilized with the bottom-most 4 Å removed from the slab. All subsequent calculations were conducted on this rigid surface. All slab calculations used a vacuum spacing of at least 15 Å normal to the surface. A single molecule was adsorbed on the surface. Various geometric configurations were examined. For dissociatively adsorbed species, it was assumed that the dissociated hydrogen atom remains chemisorbed on the surface. The vibrational frequencies of the adsorbates were evaluated within the harmonic approximation.[42] To compare to experimental results, the calculated frequencies were scaled by a factor of 0.98. This reflected the differences between the DFT calculated and experimentally observed frequencies for gas phase CO.[23]

3. RESULTS

3.1. Catalyst Characterization. Nitrogen physisorption results showed that the surface area and pore volume of niobium oxide decreased with increasing calcination temperature (Table 1). The decrease in the latter was significant

Table 1. N_2 Physisorption Results for Niobium Oxide Calcined at Different Temperatures

catalyst	BET surface area (m^2/g)	BJH pore volume (cm^3/g)	BJH pore size (nm)
NB350	109	0.17	6.4
NB400	78	0.16	8.1
NB500	34	0.15	20.2
NB600	13	0.08	33.6
NB700	6	0.02	16.9

starting at a calcination temperature of 500 °C. The average pore size of the catalysts increased with increasing calcination temperature. However, the value dropped when niobium oxide was calcined at 700 °C.

The TGA and DTA curves (Figure S1) showed an endothermic weight loss as niobic acid loses water up to 400 °C. This was followed by a sharp exothermic peak at 582 °C, indicating that crystallization has occurred. XRD patterns of the catalysts (Figure S2) revealed that NB350 and NB400 were amorphous. As the calcination temperature reached 500 °C, diffraction peaks at 22.9°, 28.7°, 36.9°, 45.9°, 50.1°, and 55.1° appeared. The same diffraction pattern was observed for NB600, but the peaks were more intense. At this stage, niobium oxide had crystallized as the T-phase, where Nb atoms are arranged either in distorted octahedra or pentagonal bipyramids.[25] For NB700, the diffraction peaks at 28.7° and 50.1° become doublets, which is attributed to octahedral NbO_6 blocks that share corners and edges with each other.[25] These results are in good agreement with other reports.[9,27,43]

Figure 1 shows the Raman spectra of the catalysts. The broad peak at 655 cm^{-1} is attributed to Nb−O−Nb vibrations in amorphous niobium oxide containing mostly distorted NbO_6 but also NbO_7 and NbO_8 polyhedra.[44] As the calcination temperature was increased, the peak blue-shifted to 694 cm^{-1}

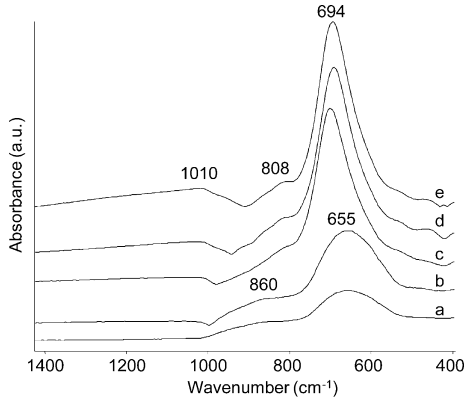

Figure 1. Raman spectra of (a) NB350, (b) NB400, (c) NB500, (d) NB600, (e) NB700.

and became sharper, indicating that some of these polyhedra were rearranged. For NB350 and NB400, a broad shoulder at 860 cm^{-1} was observed. This is assigned to Nb−O−Nb vibrations in NbO_6 octahedra.[45] As the catalyst crystallized, more octahedral cages became distorted, resulting in a red-shift to 808 cm^{-1}. The presence of NbO_4 tetrahedra was indicated by a peak at 1010 cm^{-1} that corresponds to Nb═O stretching vibrations and began to appear at 500 °C.[46]

Lewis and Brønsted acid sites were quantified by pyridine adsorption followed by IR spectroscopy (Table 2). The

Table 2. Concentrations of Lewis (LAS) and Brønsted Acid Sites (Bas) That Bind Pyridine at 150 and 350 °C on Niobium Oxide Calcined at Different Temperatures[a]

	150 °C		350 °C	
catalyst	LAS	BAS	LAS	BAS
NB350	65	40	54	26
NB400	45	29	42	22
NB500	37	8	31	5
NB600	12	1.2	10	0.9
NB700	2.6	0	1.8	0
Na^+/NB500	38	0	29	0

[a]Concentrations in μmol/g.

concentrations were obtained after heating the sample to 150 and 350 °C. The concentration of acid sites decreased with increasing calcination temperature. After calcination at 700 °C, no Brønsted acid sites were left on niobium oxide. For Na^+/NB500, the concentration of Lewis acid sites was the same as for NB500, indicating that Na^+ cations do not contribute to Lewis acidity. The absence of the pyridinium ion peak at 1540 cm^{-1} in the spectrum of Na^+/NB500 (Figure S3) shows that all Brønsted sites were successfully blocked by Na^+.[47] To understand how acidity affects acrolein formation, NB350, NB500, NB700, and Na^+/NB500 were used in this study as the catalysts have a large disparity in their acid site ratios.

The strengths of Lewis acid sites for both NB350 and NB500 were comparable (Figure 2a). For NB700, a slightly smaller fraction of the Lewis acid sites was able to retain pyridine at 350 °C. NB500 had a slightly larger fraction of strong Brønsted acid sites than NB350 (Figure 2b). This shows that NB500 possesses both strong Lewis and Brønsted acid sites even though it has a lower concentration compared to NB350.

3.2. *In-Situ* Generation of Brønsted Acid Sites. To prove that Brønsted sites can be generated from Lewis acid sites

dx.doi.org/10.1021/cs5006376 | ACS Catal. 2014, 4, 3180−3192

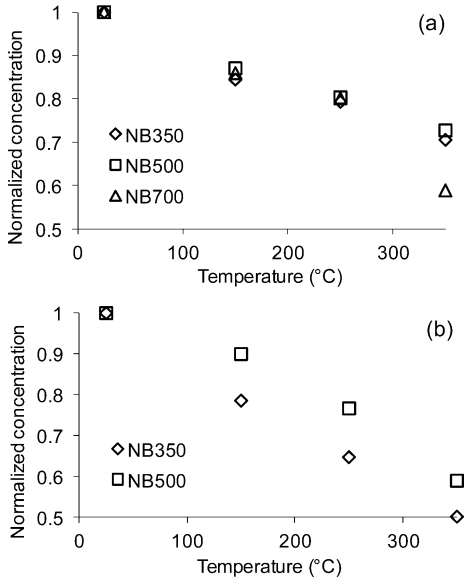

Figure 2. Relative strength of acid sites on niobium oxide calcined at different temperatures: (a) Lewis acid sites, (b) Brønsted acid sites.

in the presence of water, Na^+/NB500 was exposed to 1 mbar of water vapor at 350 °C in the FTIR transmission cell for 1 h after activation (350 °C), followed by pyridine adsorption. In a vacuum, pyridine adsorbed on Lewis acid sites (1445 cm^{-1}) can be observed, but the absence of the characteristic peak of the pyridinium ion at 1540 cm^{-1} indicates that no Brønsted sites are present (Figure 3a). In the presence of water vapor, the

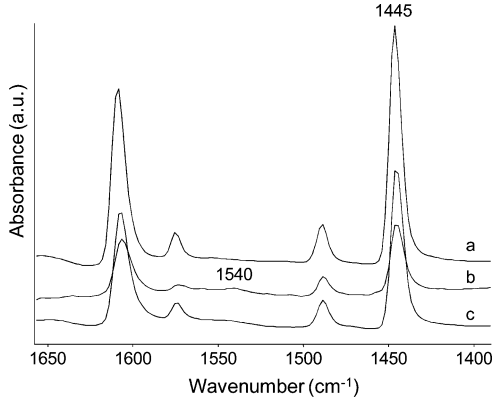

Figure 3. IR spectra of adsorbed pyridine on Na^+/NB500 at 350 °C (a) in a vacuum, (b) in the presence of 1 mbar water vapor, (c) in a vacuum after dosing 1 mbar water vapor.

concentration of active Lewis acid sites (1445 cm^{-1}) on Na^+/NB500 decreased by 59% (Figure 3b). At the same time, the formation of Brønsted acid sites (1.7 μmol/g) was observed, which corresponds to 34% of the Brønsted acid site concentration of NB500. This is attributed to the dissociative adsorption of water molecules on Lewis acid sites to form OH groups.[48] Note that the number of lost Lewis acid sites exceeds the number of Brønsted acid sites formed. This indicates that adsorption of water vapor on Lewis acid sites does not always lead to the formation of a Brønsted acid site. To ensure that Brønsted acid sites were not generated due to the removal of Na^+ by steam, the sample was exposed to 1 mbar of steam followed by evacuation and dosing with pyridine. No pyridinium ions (1540 cm^{-1}) were observed (Figure 3c).

3.3. Adsorption of Acrolein and Hydroxyacetone.

When acrolein was adsorbed on NB500, multiple bands corresponding to νC═O vibrations were observed at 1732, 1690, and 1660 cm^{-1} (Figure 4a). According to the results of

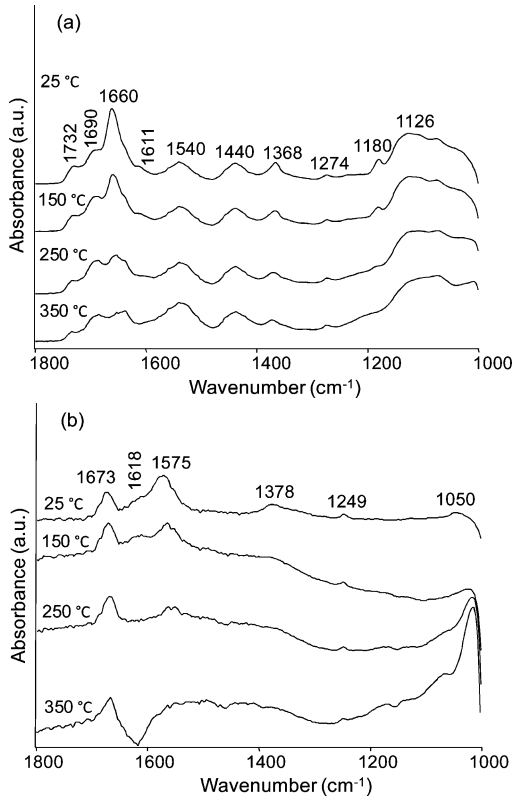

Figure 4. FTIR spectra of adsorbed oxygenates on NB500 at different temperatures: (a) acrolein, (b) hydroxyacetone.

our DFT calculations, acrolein should only have one νC═O peak (Table 3), and this is for an adsorbed molecule interacting with a Lewis acid site, giving a downshifted frequency of 1694 cm^{-1} (see Supporting Information). This lower frequency indicates a weakening of the C═O bond as a result of the interaction between the carbonyl O and Nb atom. The experimental frequency at 1732 cm^{-1} corresponds to a free carbonyl group as it is also observed in the spectrum of pure acrolein (Figure S7a), while the red-shifted frequency at 1660 cm^{-1} could be due to conjugation with the alkene group.[49] Conjugation between the carbonyl and alkene group was also observed in the spectrum of pure acrolein (Figure S7a). The alkene group also interacts with the surface (Figure 5a), giving a frequency of 1611 cm^{-1} (νC═C). Additional bands (1540 and 1126 cm^{-1}) that are not shown by DFT calculations could arise due to cyclic structures through aldehyde autocondensation[50] and the interaction between an ether group of the cyclic structure and a Nb atom. At higher temperatures, the intensity of these two bands increased, suggesting that more oligomers were formed. The alkene group, together with the νC−C band at 1611 and 1180 cm^{-1}, respectively, were not observed above 250 °C due to its weak intensities. The rest of the bands in the spectra (1440, 1368, 1274, and 1180 cm^{-1}) are close to the frequencies from DFT calculations (Table 3).

Hydroxyacetone is able to undergo tautomerization to form 1-propene-1,2-diol or 2-propene-1,2-diol. Under acidic conditions, the formation of 2-propene-1,2-diol is preferred.[51] The

dx.doi.org/10.1021/cs5006376 | ACS Catal. 2014, 4, 3180−3192

Table 3. Calculated and Experimental Frequencies of Acrolein and 2-Propene-1,2-diol Adsorbed on NB500

acrolein			2-propene-1,2-diol		
calculated/cm^{-1}	experimental/cm^{-1}	assignment	calculated/cm^{-1}	experimental/cm^{-1}	assignment
1694	1732	νC═O	1578	1575	νC═C
	1690				
	1660				
1611	1611	νC═C	1378	1378	δCH_2
1413	1440	ρCH in COH	1360		δCH_2
1337	1368	δCH_2	1318		δC−C
1277	1274	τCH	1303		τC−C
1153	1180	νC−C	1274	1249	ωCH_2
			1140		νC−C
			1061	1050	νCO

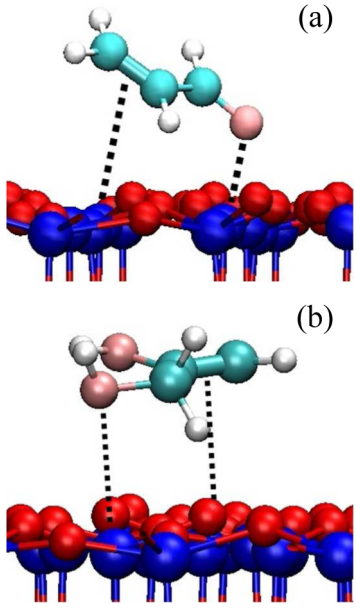

Figure 5. Structure of glycerol dehydration products adsorbed on the T-phase of Nb_2O_5 (a) acrolein, (b) 2-propene-1,2-diol. Blue, red, pink, teal, and white spheres correspond to Nb, surface O, adsorbate O, C, and H atoms, respectively.

spectrum of hydroxyacetone on NB500 contains a peak at 1575 cm^{-1} and a shoulder at 1618 cm^{-1} (Figure 4b). DFT calculations of 2-propene-1,2-diol adsorbed on NB500 indicated that the frequency at 1575 cm^{-1} corresponds to νC═C vibration and that the functional group interacts with an unsaturated Nb atom (Table S1). Thus, the shoulder at 1618 cm^{-1} could be assigned as the νC═C vibration of 1-propene-1,2-diol. The frequencies calculated for the adsorption of 2-propene-1,2-diol are compared with experimental results (Table 3). The band at 1673 cm^{-1} is attributed to νC═O of the ketone form interacting with the surface compared to its free νC═O mode at 1718 cm^{-1} (Figure S7b).[52] In contrast to pure hydroxyacetone, which has a νC−O band at 1076 cm^{-1}, the enol displayed a νC−O frequency at 1050 cm^{-1} when it is adsorbed on the surface. DFT calculations showed that the primary hydroxyl group forms a strong interaction with a coordinatively unsaturated Nb atom (Figure 5b). On the basis of the spectroscopic data and DFT calculations it was not possible to determine whether this interaction of the primary alcohol group led to its dissociation or not (Table S1 and Figure S5). The alkene group interacts with another Nb atom, giving a frequency at 1575 cm^{-1}. However, the secondary hydroxyl group does not interact with the surface when the enol is adsorbed on the surface. Moreover, a surface interaction of the secondary alcohol group should blue shift the νCO vibration to the range of 1070−1150 cm^{-1},[24] and no peak was observed in this part of the spectrum. The frequencies for adsorbed acrolein and 2-propene-1,2-diol can be used to identify the dehydration products from the *in situ* FTIR experiments.

3.4. Formation of Surface Species from Glycerol on NB350. Pure glycerol has bands at 1454 and 1413 cm^{-1}, due to δCH_2 and δOH vibrations, while bands at 1326 and 1209 cm^{-1} are assigned to ρOH and ωCH_2 vibrations (Figure 6Ai).[53,54] When 2 wt % of glycerol (equivalent to one monolayer) was impregnated on NB350, these vibrational modes appeared at 1458, 1413, 1326, and 1208 cm^{-1}, respectively (Figure 6Aa). Pure glycerol has a primary and secondary νC−O vibration at 1029 and 1108 cm^{-1}, respectively (Figure 6Ai), and significant changes were observed in this region. For a monolayer or 2.0 wt % of glycerol impregnated on NB350 at RTP (Figure 6A), peaks were observed at 1045 cm^{-1}, 1108 cm^{-1}, and 1140 cm^{-1}. Upon evacuation, the shoulder at 1140 cm^{-1} became more intense, the peak at 1108 cm^{-1} vanished, and a peak at 1093 cm^{-1} appeared (Figure 6Ab). In addition, the band at 1045 cm^{-1} became a shoulder. In agreement with earlier studies, the peaks at 1093 and 1045 cm^{-1} are attributed to the stretching vibration of the primary C−O bonds of glycerol that are part of a bridging alkoxy bonds and a nondissociative Lewis acid−base interaction with the surface, respectively (inset of Figure 6A).[23,24] The band at 1140 cm^{-1} is assigned to the νC−O vibration of the secondary OH group of glycerol forming a hydrogen bond to a basic oxygen atom on the metal oxide surface.[23,24] This indicates that some water molecules were desorbed from the surface after evacuation, allowing a larger number of OH groups from glycerol molecules to interact with the Lewis acid sites and surface oxygen atoms.

In addition to the bands that are attributed to adsorbed glycerol, a number of bands were observed in every spectrum of glycerol loaded NB350. The region between 1500 and 1200 cm^{-1} contains multiple convoluted bands, but some of these may indicate the presence of acrolein (1446, 1370, and 1270 cm^{-1}) and 2-propene-1,2-diol (1370 and 1244 cm^{-1}), respectively (Figure 6A).

A strong band at 1630 cm^{-1} is attributed to the δOH of coadsorbed water. Upon increasing the temperature, this peak decreased in intensity and red-shifted toward 1610 cm^{-1} as water began to desorb from the surface (Figure 6Ab−h). A reference experiment without adsorbed glycerol also showed a red shift to 1610 cm^{-1} as the amount of water on the surface

dx.doi.org/10.1021/cs5006376 | ACS Catal. 2014, 4, 3180−3192

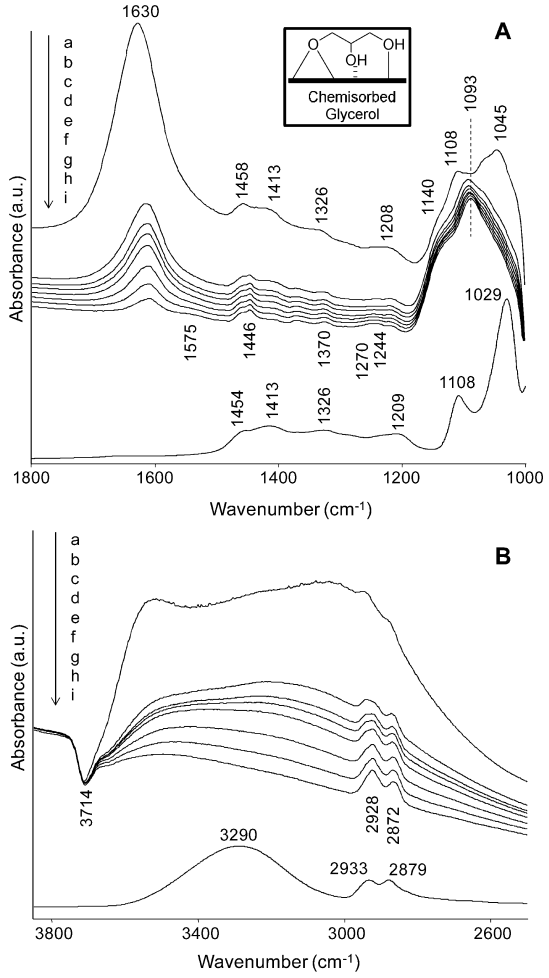

Figure 6. FTIR spectra of 2 wt % glycerol on NB350 at (a) RTP, (b) RTHV, (c) 100 °C HV, (d) 150 °C HV, (e) 200 °C HV, (f) 250 °C HV, (g) 300 °C HV, (h) 350 °C HV, and (i) pure glycerol. (A) Between 1800 and 1000 cm^{-1}. (B) Between 3800 and 2600 cm^{-1}. Inset: Scheme of chemisorbed glycerol.

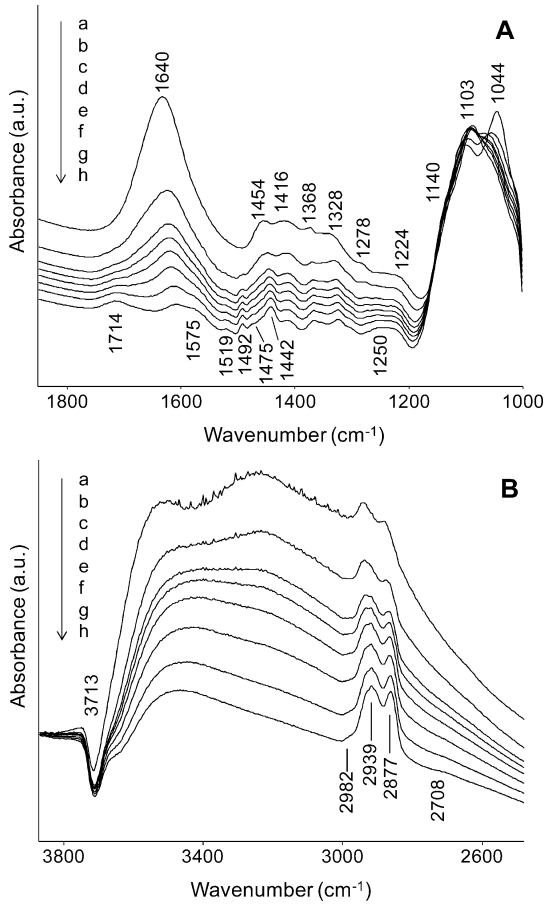

Figure 7. FTIR spectra of 3 wt % glycerol on NB350 at (a) RTP, (b) RTHV, (c) 100 °C HV, (d) 150 °C HV, (e) 200 °C HV, (f) 250 °C HV, (g) 300 °C HV, (h) 350 °C HV. (A) Between 1800 and 1000 cm^{-1}. (B) Between 3800 and 2600 cm^{-1}.

decreases (Figure S8). Additionally, a small band at 1575 cm^{-1} was observed. This peak is characteristic of a νC═C vibration. Based on the position of this band and the much higher intensity of the νC═C band of adsorbed 2-propene-1,2-diol compared to acrolein, this peak is assigned to the νC═C band of 2-propene-1,2-diol. When the temperature reached 350 °C, unreacted glycerol, acrolein and 2-propene-1,2-diol were still present on the surface. Note that these surface species were also present when the experiment was performed in the presence of 1 mbar of water (Figure S9).

The asymmetric and symmetric νCH_2 bands of pure glycerol (2933 and 2879 cm^{-1}) were slightly red-shifted, and they were observed at 2928 and 2872 cm^{-1}, respectively (Figure 6B). The negative peak at 3714 cm^{-1} (Figure 6Ba–h) indicates that the hydroxyl groups on NB350 are perturbed, possibly interacting with the adsorbed species.[45]

When more than a monolayer of glycerol (3.0 wt %) was impregnated on NB350 and the sample was heated up, additional small bands at 2708, 1519, 1492, and 1475 cm^{-1} were observed (Figure 7). The weak band at 2708 cm^{-1} is assigned to the νCH vibration of the aldehyde group of acrolein.[55] This band was not observed for 2.0 wt % glycerol on NB350 as the amount of acrolein formed on the surface was not large enough for it to be visible. The bands at 1519, 1492, and 1475 cm^{-1} were observed from 100 °C, and their intensity increased steadily with increasing temperature (Figure 7A), suggesting that they correspond to reaction products. In some reports, these frequencies have been assigned as νC═C and δCH of coke species.[56,57] The peaks at 1519 and 1492 cm^{-1} correspond to vibrations of two different types of aromatic rings.[58,59] Bands between 1500 and 1525 cm^{-1} usually arise due to aromatic rings with multiple electron donating substituents, while the peak at 1492 cm^{-1} could be due to a monosubstituted aromatic ring. The shoulder at 1475 cm^{-1} is attributed to a combination band of νCC_{ring} and δOH.[60] The presence of a methyl group attached to an aromatic ring was excluded due to the absence of a triplet band around 1475 cm^{-1}.[55] Similar bands at 1519 and 1475 cm^{-1} are observed in the spectrum of hydroquinone,[61] while the band at 1492 cm^{-1} could be due to the presence of benzene or phenol. For convenience, these two surface species are collectively termed as monoaromatics. Aromatic rings possess another vibrational mode due to conjugated νCC that exist around 1600 cm^{-1}. However, this weak band was not resolved as this part of the spectrum is dominated by the intense peak corresponding to the δOH vibration of water.

Under RTHV, the secondary and primary νCO modes of pure glycerol (1103 and 1044 cm^{-1}) were still observed as there was more than a monolayer of glycerol present (Figure 7Aa). The intensity of the primary νCO mode gradually decreased as

dx.doi.org/10.1021/cs5006376 | ACS Catal. 2014, 4, 3180–3192

the temperature increased and the alkoxy modes at 1140 and 1054 cm^{-1} became visible (Figure 7Ah). This indicates that a large fraction of glycerol on the surface was converted or desorbed until less than one monolayer was present. Similar to the sample with 2.0 wt % glycerol on NB350, the band corresponding to the νC═C vibration of 2-propene-1,2-diol (1575 cm^{-1}) increased in intensity at higher temperatures. The broad νC═O band of adsorbed acrolein (1714 cm^{-1}) also became noticeable as the water peak at 1640 cm^{-1} decreased in intensity, while its other vibrational modes at 1442 cm^{-1} (rCHO), 1368 cm^{-1} (δCH_2), and 1278 cm^{-1} (τCH) were still present. At higher temperatures, a small shoulder at 2988 cm^{-1} was observed while the $\nu_{asym}CH_2$ becomes broader (Figure 7B). This corresponds to the rise of the asymmetric and symmetric νCH_2 of alkene groups in acrolein and 2-propene-1,2-diol, which are red-shifted relative to 3062 and 2990 cm^{-1} as the alkene groups are interacting with the surface.[62] As the temperature reached 350 °C, surface species due to unreacted glycerol, acrolein, 2-propene-1,2-diol, and monoaromatics were present on the surface.

On the basis of previous reports,[6,14] the possible formation of other products was considered. Specifically, 1,3-propenediol, 3-hydroxypropionaldehyde, acetaldehyde, and formaldehyde deserve attention. The vibrational spectrum of adsorbed 1,3-propenediol was modeled by DFT calculations (Table S2). Most bands corresponding to this species were in the range of 1000 to 1400 cm^{-1}, which also contains multiple peaks from other species making a positive identification impossible. The region of C═C stretching bands is slightly better resolved. This region of spectrum can be fitted with peaks corresponding to the νC═C of 2-propene-1,2-diol (1575 cm^{-1}) and adsorbed water (1610 cm^{-1}) without requiring a contribution at the expected νC═C frequency of 1585 cm^{-1} for 1,3-propenediol. On the basis of these observations, it is suggested that 1,3-propenediol was not present on the surface in a measurable concentration. 3-Hydroxypropionaldehyde was not expected to exist as it is a very reactive and unstable molecule above 4 °C.[12,63−65] It is possible that the $\nu_{asym}CH_3$ band of acetaldehyde contributes to the shoulder around 2985 cm^{-1}.[55] However, the shoulder is rather small and contains a contribution from the $\nu_{asym}CH_2$ of 2-propene-1,2-diol. Furthermore, the νC═O region of the spectrum was adequately fitted with a single peak leading to the assumption that acrolein is the only carbonyl present on the surface. No characteristic signals were observed for formaldehyde or its decomposition product CO.

3.5. Formation of Surface Species on NB500. The spectrum of 3.0 wt % glycerol on NB500 at room temperature and ambient pressure also contained peaks that cannot be attributed to glycerol or water (Figure 8A). As described above, these bands indicate the presence of adsorbed acrolein (1712, 1442, 1367, and 1278 cm^{-1}) and 2-propene-1,2-diol (1575, 1367, and 1256 cm^{-1}). At room temperature and ambient pressure, the νC═O mode of acrolein and the νC═C mode of 2-propene-1,2-diol are only observed as shoulders at 1712 and 1575 cm^{-1}, respectively. However, the peak became more resolved upon evacuation (Figure 8A). As the temperature increased, the intensity of the bands corresponding to dehydration products increased in intensity (Figure 8Ab−h). Bands due to glycerol (1454, 1415, 1331, 1222, 1110, and 1046 cm^{-1}) and water (1640 cm^{-1}) decreased in intensity. At temperatures of 250 °C and above, a new band was observed at 2694 cm^{-1} (Figure 8B), which is assigned to the Fermi resonance of the νCH of the aldehyde group in acrolein with

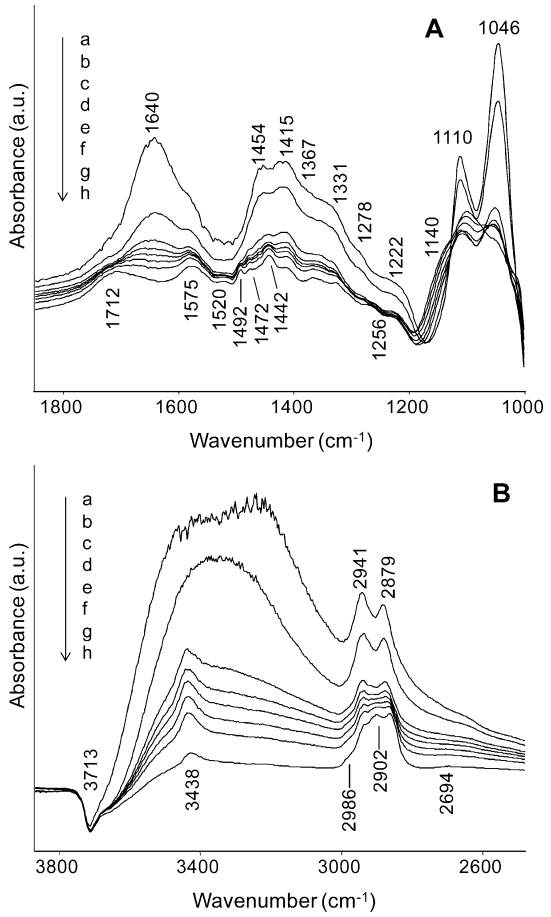

Figure 8. FTIR spectra of 3 wt % glycerol on NB500 at (a) RTP, (b) RTHV, (c) 100 °C HV, (d) 150 °C HV, (e) 200 °C HV, (f) 250 °C HV, (g) 300 °C HV, (h) 350 °C HV. (A) Between 1800 and 1000 cm^{-1}. (B) Between 3800 and 2600 cm^{-1}.

the ρCOH vibration at 1440 cm^{-1}.[55] Bands corresponding to monoaromatics (1520, 1492, and 1472 cm^{-1}) were visible and distinct starting at 100 °C.

The modes from the νC−O vibrations of a bridging alkoxy group at 1100 cm^{-1} and the alcohol group engaged in the Lewis acid−base interaction at 1046 cm^{-1} became more resolved at higher temperatures as the amount of nonchemisorbed glycerol on the surface decreased. The perturbation of hydroxyl groups can be identified by the negative peak at 3713 cm^{-1} (Figure 8B). The band at 3438 cm^{-1} could be due to hydroxyl groups that are engaged in hydrogen bonding interactions, and they could be located in pores which are inaccessible. Note that this band was not observed for NB350. These hydroxyl groups could be formed after the oxide has crystallized. The $\nu_{asym}CH_2$ and $\nu_{sym}CH_2$ modes of glycerol at 2941 and 2879 cm^{-1} remained unchanged, while the $\nu_{asym}CH_2$ and $\nu_{sym}CH_2$ vibrational modes of alkene groups began to appear from 150 °C at 2986 and 2902 cm^{-1}. Similar to the sample with 3.0 wt % glycerol on NB350, the remaining surface species at 350 °C were glycerol, acrolein, hydroxyacetone enol, and monoaromatics.

3.6. Formation of Surface Species on NB700. For NB700 impregnated with 3.0 wt % of glycerol, only vibrational modes corresponding to nonchemisorbed glycerol were observed under RTHV at 1458, 1418, 1333, 1217, 1110, and 1042 cm^{-1} (Figure 9A). Upon increasing the temperature, the

dx.doi.org/10.1021/cs5006376 | ACS Catal. 2014, 4, 3180−3192

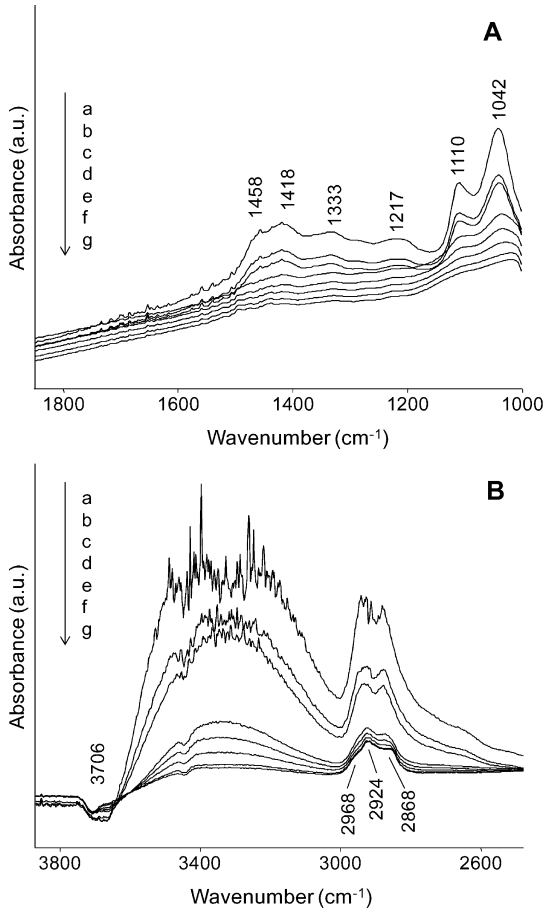

Figure 9. FTIR spectra of 3 wt % glycerol on NB700 at (a) RTHV, (b) 100 °C HV, (c) 150 °C HV, (d) 200 °C HV, (e) 250 °C HV, (f) 300 °C HV, (g) 350 °C HV. (A) Between 1800 and 1000 cm^{-1}. (B) Between 3800 and 2600 cm^{-1}.

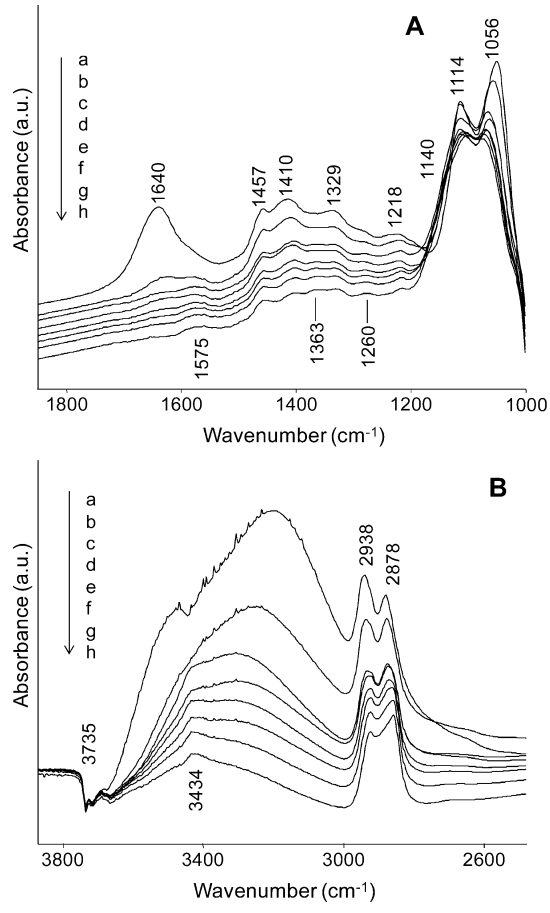

Figure 10. FTIR spectra of 3 wt % glycerol on Na^+/NB500 at (a) RTP, (b) RTHV, (c) 100 °C HV, (d) 150 °C HV, (e) 200 °C HV, (f) 250 °C HV, (g) 300 °C HV, (h) 350 °C HV. (A) Between 1800 and 1000 cm^{-1}. (B) Between 3800 and 2600 cm^{-1}.

intensity of these bands decreased, and they were no longer observed as the temperature reached 350 °C (Figure 9Ab–g). However, the $\nu_{asym}CH_2$ and $\nu_{sym}CH_2$ vibrational modes were still present at 2924 and 2868 cm^{-1}, respectively (Figure 9B). In addition, a shoulder at 2968 cm^{-1} appeared at higher temperatures. The perturbation of hydroxyl groups can still be observed by the negative peak at 3706 cm^{-1}. It is suggested that the remaining νCH_2 vibrations could be due to hydrocarbons that resulted from the cracking of glycerol.[11]

3.7. Formation of Surface Species on Na^+/NB500. Impregnation of Na^+/NB500 with 3.0 wt % glycerol at RTP resulted in the appearance of characteristic bands for adsorbed glycerol at 1457, 1410, 1329, 1218, 1114, and 1056 cm^{-1} (Figure 10A). Upon evacuation, the band at 1640 cm^{-1} (δOH of water) significantly decreased in intensity due to the absence of hydrophilic Brønsted acid sites, revealing a weak shoulder at 1575 cm^{-1} (Figure 10Ab). In addition, weak bands at 1363 cm^{-1} (δCH_2) and 1260 cm^{-1} (ωCH_2) were observed, which are assigned to 2-propene-1,2-diol. It is important to note that the intensity of these characteristic peaks for adsorbed propene-diol was much lower than in the case of NB500. The characteristic bands for adsorbed acrolein were not observed. The $\nu_{asym}CH_2$ and $\nu_{sym}CH_2$ vibrational modes of glycerol were visible at 2938 and 2878 cm^{-1}, respectively. As the temperature increased, the band at 2878 cm^{-1} broadened and increased in intensity (Figure 10Bb–h). The perturbation of hydroxyl groups was observable by the 3735 cm^{-1} negative peak, while the band at 3434 cm^{-1} could be assigned to another set of hydroxyl groups. Bands from acrolein and monoaromatics were not observed as the temperature increased to 350 °C (Figure 10Ab–h). Only glycerol and 2-propene-1,2-diol were present on the surface by 350 °C.

4. DISCUSSION

4.1. Formation of Multidentate Species between Glycerol and Lewis Acid Sites on Niobium Oxide. Glycerol is able to chemisorb to the surface of various metal oxides (i.e., Al_2O_3, TiO_2, ZrO_2, CeO_2) when strong Lewis acid sites are present.[23,24] In this process, the proton of one of the primary alcohol groups dissociates to form a bridging alkoxy bond with two coordinatively unsaturated metal atoms, while the other primary OH group coordinates nondissociatively to one of these metal atoms. The remaining secondary OH group may form a hydrogen bond to a basic surface oxygen atom, but this interaction can be inhibited by coadsorbed water or CO_2. Over Al_2O_3, TiO_2, and ZrO2, this surface species was dominant, and there was no clear evidence for any other ones.[23,24] However, in the case of CeO_2, additional νC–O bands were observed upon evacuation due to interactions of glycerol with oxygen vacancies.[24]

The IR spectra in the present study (Figures 6–10) show that glycerol is able to form the same multidentate surface species on all of the niobium oxide catalysts, except for NB700,

dx.doi.org/10.1021/cs5006376 | ACS Catal. 2014, 4, 3180–3192

which possesses very few Lewis acid sites. It was reported that Lewis acid sites of sufficient strength are needed for polyols to form alkoxy bonds with the metal oxide surface.[24] Chemisorbed glycerol was still observed on the rest of the catalysts at 350 °C, indicating a considerable strength of the surface reactions (Figures 6−10).

Since glycerol dehydration can be performed in the gas phase in the presence of steam, it is necessary to verify whether the multidentate surface species is stable in the presence of water vapor. For experiments in the presence of 1 mbar water vapor, there were no changes in the FTIR spectrum compared to high vacuum conditions (Figure S9). The same heating procedure for glycerol dehydration was also used in the presence of 1 mbar water vapor, and there were no changes compared to Figure 6. These observations suggest that the alkoxy bonds on niobium oxide are stable at high temperatures in the presence of water vapor. In related studies, it was reported that similar surface species are stable on Pt/γ-Al_2O_3 catalysts and that hydrolytic decay of the alumina support can be stopped in the presence of multidentate deposits from biomass-derived oxygenates.[66,67]

During the formation of the chemisorbed surface species, the chemical bonds in the adsorbing molecule are polarized. Specifically, the blue shift of the bands corresponding to C−O stretching vibrations indicates that electron density is transferred from the carbon atom to the oxygen atom resulting in a larger dipole moment and higher frequency. Copeland et al. found a positive linear correlation between the frequencies of the νC−O vibrations of the bridging alkoxy group (α) and the alcohol group engaged in a Lewis acid−base interaction (γ) with the electronegativity of the surface metal atoms.[24] Niobium has an electronegativity of 1.23, and the bands corresponding to the α and γ interactions appear at 1095 and 1058 cm^{-1}, respectively.[68] These numbers fit the linear trend with other metal oxides such as γ-Al_2O_3, TiO_2, ZrO_2, and CeO_2.[24] It is interesting to note that the observed shifts for glycerol on niobia were smaller than the corresponding values on γ-Al_2O_3 and TiO_2 and comparable to the ZrO_2 samples, indicating a limited extent of polarization of this surface species on niobia.

4.2. Role of Lewis and Brønsted Sites in the Dehydration of Glycerol. Two pathways for dehydration of glycerol have been discussed in the literature.[10,12] The first pathway proceeds via the dehydration of a terminal OH group to form an intermediate enol (2-propene-1,2-diol), which easily tautomerizes to the thermodynamically favored hydroxyacetone.[10] The latter is a stable product. The second pathway proceeds via the formation of 3-hydroxypropionaldehyde by dehydration of the secondary OH group. The intermediate can either undergo a retroaldol reaction to form acetaldehyde and formaldehyde, or a second dehydration step to form acrolein.[12]

The conversion of glycerol to other surface species by dehydration was observed at room temperature on all of the niobium oxide catalysts except for NB700 (Figures 6−10). Surface species like acrolein and 2-propene-1,2-diol were formed on NB350 and NB500, while only a small amount of the latter was observed on Na^+/NB500. Pyridine adsorption followed by FTIR spectroscopy revealed that NB700 does not possess any Brønsted acid sites and only very few Lewis acid sites (Table 2). Furthermore, it has a low surface area (Table 1). Due to these reasons, glycerol is not able to bind to the surface to any measurable extent.

As shown in the previous section, Lewis acid sites readily chemisorb glycerol forming cyclic surface species, which involve strong surface interactions of both primary alcohol groups. The resulting polarization renders the primary alcohol group susceptible to dehydration (Scheme 1). Considering the

Scheme 1. Role of Lewis (LAS) and Brønsted (BAS) Acid Sites in the Dehydration of Glycerol

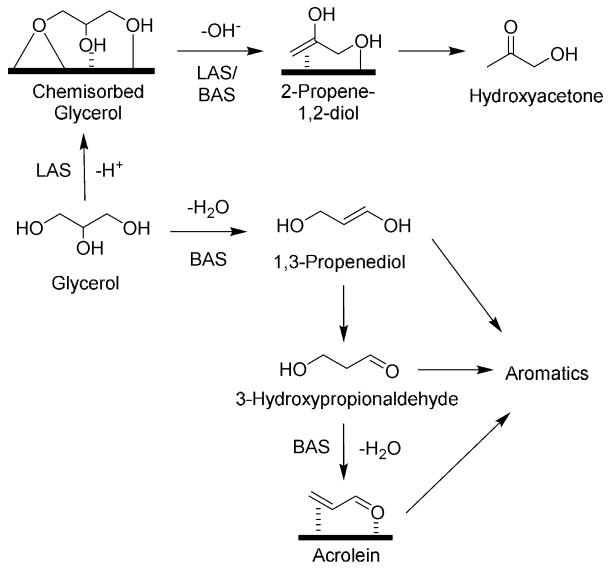

preferential interaction of glycerol with Lewis acid sites, it is not surprising that the characteristic IR bands of 2-propene-1,2-diol were much stronger than the ones of acrolein when the loading on NB350 was limited to one monolayer (Figure 6). Moreover, 2-propene-1,2-diol was the only identifiable product from glycerol dehydration on Na^+/NB500, which only contained Lewis acid sites (Figure 10). It is interesting to point out that glycerol adsorbed on the Lewis acid sites of niobia was dehydrated, whereas this reaction was not observed at room temperature for the comparable surface species on Al_2O_3 and ZrO_2, which are polarized to the same extent or more strongly (vide supra).[24] The key differences between these materials is the presence of Brønsted acid sites in Nb_2O_5 (Table 2), which were absent in Al_2O_3 and ZrO_2.[24] Thus, it is concluded that dehydration of glycerol adsorbed on the Lewis acid sites of niobia involves the participation of nearby Brønsted acid sites. Further evidence for the involvement of Brønsted acid sites in the formation of 2-propene-1,2-diol is obtained from the reduced amount of 2-propene-1,2-diol on the surface of Na^+/NB500 (Figure 10) compared to NB500 (Figure 8). A small amount of Brønsted acid sites could be generated on Na^+/NB500 during the impregnation procedure in the presence of an aqueous solution, which explains why dehydration products are still detected. Moreover, Nimlos et al. reported that the barrier for glycerol dehydration is significantly lowered in the presence of Brønsted acids, making it more susceptible to decomposition at much lower temperatures.[19]

Interestingly, 2-propene-1,2-diol was observed as a product of dehydration while its ketone form (i.e., hydroxyacetone) was not present on the surface (Scheme 1). It is suggested that 2-propene-1,2-diol can be stabilized by formation of a bidentate surface species. DFT calculations indicated that the enol can interact with the surface through its primary alcohol group as well as the π-system of the olefinic double bond (Figure 5b).

dx.doi.org/10.1021/cs5006376 | ACS Catal. 2014, 4, 3180−3192

The calculated vibrational frequencies for this species are in good agreement with the experimental spectra (Table 3). Specifically, the primary OH group of the enol interacts nondissociatively with a Lewis acid metal atom, giving a frequency of 1050 cm^{-1}. This frequency also corresponds to the νC−O vibration of a primary alcohol group in glycerol that is engaged in a Lewis acid−base interaction with the surface. Since this interaction is the weaker one of the two interactions of the primary alcohol groups in glycerol with the Lewis acid sites, its continued existence indicates that the eliminated alcohol group might be the one forming the bridging alkoxy bond to the Lewis acid site. After the primary hydroxyl group is dehydrated, the olefinic π-system that was formed interacts with a Lewis acid site (Figure 5b). However, the secondary alcohol group of 2-propene-1,2-diol does not interact with the surface. In agreement with the observation of this surface species, a previous study indicated that the formation of bidentate surface species is much more favorable when there is sufficient spatial separation between the functional groups.[23] In contrast, bidentate surface species involving functional groups on vicinal carbon atoms (e.g., hydroxyacetone) are strongly strained and, thus, less stable. Subsequent to the formation of 2-propene-1,2-diol, the molecule can desorb from the surface and tautomerize to its ketone form (Scheme 1).[18] The barrier for tautomerization is lower than dehydration, and it should occur easily.[19]

It is important to note that 2-propene-1,2-diol cannot be converted to acrolein. The elimination of the secondary alcohol group would result in the formation of highly unstable adjacent C=C double bonds. Moreover, 2-propene-1,2-diol was found to interact with the niobia in a way that the secondary alcohol is pointing away from the surface, preventing its interaction with acid sites.

The formation of hydroxyacetone has been a subject of debate, but understanding the role of Lewis and Brønsted acid sites in the dehydration of glycerol can provide an explanation for the observations in the present study and previous ones. Alhanash et al. suggested that only a terminal alcohol group of glycerol is able to interact with two oxo-bridged metal atoms in heteropolyacids due to steric constraint. The alcohol group is dehydrated in a concerted manner, resulting in the conversion of the oxo-bridged metal atoms to two metal hydroxyl groups.[13] However, no direct evidence was provided for this mechanism, and the results can be explained equally well with the formation of bidentate cyclic surface species as described above. Kinage et al. proposed a different mechanism for the formation of hydroxyacetone over CeO_2, Al_2O_3, ZrO_2, and Ga_2O_3 involving dehydrogenation, dehydration, and rehydrogenation over basic sites.[69] However, all of the catalysts used in that study are Lewis acidic,[24,70] and it was shown that the bidendate surface species described in section 4.1 were also abundant surface species on CeO_2, Al_2O_3, and ZrO_2.[24]

As mentioned above, the formation of acrolein requires the secondary alcohol group of glycerol to be eliminated first forming 1,3-propenediol. In the absence of steric factors, this pathway is intrinsically favored over Brønsted acid sites as the secondary carbenium ion intermediate is more stable compared to the primary carbenium ion formed from during the elimination of the terminal OH group.[71] The primary dehydration product of this reaction, 1,3-propenediol, can tautomerize to 3-hydroxypropionaldehyde, which can be converted to acrolein in a thermodynamically favorable second dehydration step, which may occur with or without the involvement of a Brønsted acid site.[11,19,72] Suprun et al. used 3-hydroxypropionaldehyde as a reactant, and they obtained 100% conversion with a high yield of acrolein.[14] Note that direct dehydration of 1,3-propenediol would result in the formation of unstable adjacent double bonds. While it is possible that the corresponding enol, 1,3-propenediol, is stabilized by interacting with the surface of niobia, the data in the present study do not provide evidence for measurable quantities of this species on the surface.

High selectivities for the formation of acrolein were reported over Brønsted acidic zeolites.[21,73] Yoda and Ootawa proposed that the dehydration of the secondary alcohol group of glycerol is catalyzed by a Brønsted acidic bridging hydroxyl group.[21] This reaction results in the formation of an alkoxy species, which is converted to acrolein in a sequence of desorption, readsorption, and dehydration steps. Unfortunately, no direct evidence for the intermediates in this sequence could be obtained due to the strong absorption of the zeolite below 1300 cm^{-1}.[74] Wang et al. suggested that Lewis acid sites in ZSM-5 could enhance the formation of acrolein in a cooperative mechanism.[73] To achieve such a cooperative effect, the Lewis acid sites would have to be in the direct vicinity of a Brønsted acid site. Taking the spatial constraints in a zeolite cage into account, it is unlikely that the multidentate species described in the present study (vide supra) can be formed in such an environment. Consequently, only Lewis acid sites outside the zeolite are expected to favor the formation of hydroxyacetone.

Using the results of the reactivity study obtained by Chai et al., who used the same synthesis procedure for niobia catalysts to dehydrate glycerol vapor at 315 °C,[9] a strong correlation between the acid site ratio and selectivity is obtained (Figure 11). The selectivities to hydroxyacetone and acrolein increase linearly with the ratio of Lewis and Brønsted sites, respectively. An extrapolation of the curve for hydroxyacetone (Figure 11a) leads to an intercept of 9.4% selectivity, which is likely due to noncatalytic dehydration at the reaction temperature. The curve for acrolein selectivity has an intercept at 29.6%

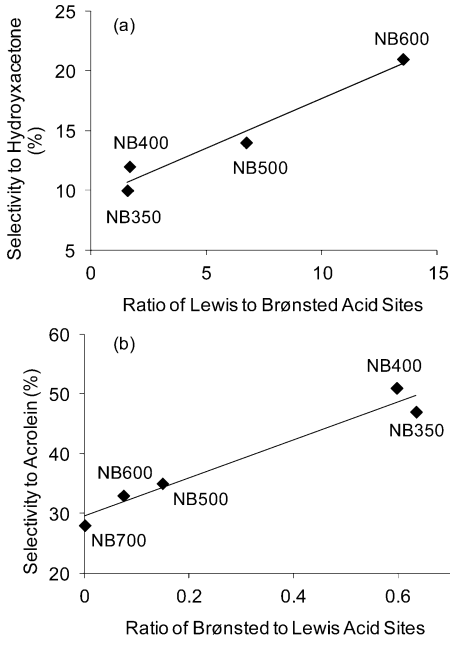

Figure 11. Correlation between (a) selectivity to hydroxyacetone and ratio of Lewis to Brønsted acid sites, (b) selectivity to acrolein and ratio of Brønsted to Lewis acid sites.

dx.doi.org/10.1021/cs5006376 | ACS Catal. 2014, 4, 3180−3192

selectivity (Figure 11b). This is attributed to the transformation of Lewis to Brønsted acid sites in the presence of steam as shown in section 3.2.[13,75] This correlation supports the proposed reaction network, in which Lewis acid sites activate primary C−O bonds of glycerol to form 2-propene-1,2-diol, while Brønsted acid sites are involved in the formation of acrolein (Scheme 1).

4.3. Formation of Monoaromatics. One of the main challenges in glycerol dehydration is deactivation due to coke formation for all of the catalysts that have been studied.[6] A possible strategy is promoting the catalyst with Pt group metal and cofeeding of hydrogen.[13] However, this method will increase the costs of the catalyst and operations. Another possibility to avoid coke formation is to cofeed oxygen.[76,77] However, the presence of oxygen could also promote the conversion of the desired products in side reactions. In a different approach, Corma et al. used an FCC type reactor where the catalyst can be continuously separated and regenerated.[11] Reports in the literature have also shown that a large pore volume can promote condensation reactions and the formation of coke.[78,79]

Our results show that some of the acid sites remain occupied by unreacted glycerol and its dehydration products at 350 °C (Figures 6−10). In addition, the formation of monoaromatics was observed when more than a monolayer of glycerol was impregnated and dehydrated on the surface of NB350 and NB500, suggesting that multimolecular reactions have occurred because at least two glycerol molecules are needed to form a monoaromatic compound. These multimolecular reactions are avoided when less than a monolayer of glycerol was present on the surface. The same reactions are also avoided in the absence of Brønsted acid sites on Na^+/NB500 even when there is more than a monolayer of glycerol present. This shows that either Brønsted acid sites play a critical role in the formation of aromatics and/or that products from Brønsted acid catalyzed dehydration (i.e., 3-hydroxypropionaldehyde, 1,3-propenediol, acrolein) are key intermediates for the formation of the aromatics (Scheme 1). The reaction path to aromatics could consist of dehydration, dehydrogenation, and cyclization reactions of carbocation intermediates.[80]

Since hydroxyacetone by itself is unreactive in the presence of Brønsted acid sites,[13] the formation of monoaromatics must involve 1,3-propenediol, 3-hydroxypropionaldehyde and/or acrolein as intermediates (Scheme 1). Studies done on the gas phase dehydration of glycerol at high temperature used an aqueous glycerol feed ranging from 10 to 85 wt %.[2,9−15] The presence of monoaromatics on the surface eventually results in the formation of coke and deactivation of the catalysts.[80] It was reported that hydroquinone, which could be one of the monoaromatic compounds present in this study, enhances the rate of coke formation by undergoing condensation.[61]

Based on the present results it is suggested that the formation of monoaromatics can be hindered as long as there is less than a monolayer of glycerol on the surface of the catalyst. Thus, using a small concentration of glycerol feed can help to prevent deactivation. However, this would shift the product distribution from acrolein to hydroxyacetone, which is usually considered the less desirable product. Alternatively, the presence of steam could aid in the desorption of the dehydration products.

5. CONCLUSIONS

Glycerol can chemisorb on strong Lewis acid sites on niobia forming a multidentate surface species. The proton of one of the primary alcohol groups dissociates to form a bridging alkoxy bond with two coordinatively unsaturated metal atoms, while the other primary alcohol group coordinates nondissociatively to one of these metal atoms. The secondary alcohol group can form a hydrogen bond to a basic oxygen atom on the surface. In the absence of Brønsted acidic protons, these alkoxy bonds are stable in the presence of water vapor and at high temperatures. However, the primary C−O bonds are polarized, and in the presence of an acidic proton, one of the primary hydroxyl groups is dehydrated to form 2-propene-1,2-diol, which can desorb and tautomerize to hydroxyacetone. When glycerol interacts with a Brønsted acid site without steric constraints, the dehydration of the secondary alcohol group is strongly preferred due to the higher stability of the corresponding carbenium ion that is formed as the transition state. This reaction forms 1,3-propenediol, which tautomerizes to 3-hydroxypropionaldehyde, an unstable intermediate that undergoes a second acid-catalyzed or thermal dehydration step to yield acrolein. The involvement of Lewis and Brønsted acid sites in different dehydration pathways is supported by the linear correlation between the selectivity to hydroxyacetone and acrolein, and the ratio of the concentrations of Lewis and Brønsted acid sites, respectively. However, this model may not be applicable to other catalytic systems with different porous constraints. Brønsted sites are also involved in multimolecular reactions, resulting in the formation of coke and catalyst deactivation.

■ ASSOCIATED CONTENT

Ⓢ Supporting Information

TGA/DTA curves of niobic acid, XRD diffractograms of niobium oxide, IR difference spectra of pyridine adsorbed on Na^+/NB500, FTIR spectra of 2 wt % glycerol on NB350 in the presence of 1 mbar water vapor. This material is available free of charge via the Internet at http://pubs.acs.org.

■ AUTHOR INFORMATION

Corresponding Author

*E-mail: carsten.sievers@chbe.gatech.edu.

Funding

U.S. Department of Energy grant DE-AC36-08-GO28308.

Notes

The authors declare no competing financial interests.

■ ACKNOWLEDGMENTS

The Renewable Bioproducts Institute is acknowledged for the use of its facilities. We thank John Copeland and Pranjal Kalita for experimental assistance and fruitful discussions. Funding from the Georgia Institute of Technology and the U.S. Department of Energy is gratefully acknowledged. The authors would like to thank CBMM for providing niobic acid.

■ ABBREVIATIONS

DFT, density functional theory; FTIR, Fourier transform infrared; BET, Brunauer−Emmett−Teller; BJH, Barrett−Joyner−Halenda; TGA, thermalgravimetric analysis; DTA, differential thermal analysis; HV, high vacuum; MCT/A, mercury cadmium telluride antimonide; RTP, room temperature and pressure; ν, stretching vibration; τ, twisting vibration; ω, wagging vibration; δ, bending vibration; ρ, rocking

REFERENCES

(1) Zhu, C. J.; Chiu, S.; Nakas, J. P.; Nomura, C. T. *J. Appl. Polym. Sci.* **2013**, *130*, 1−13.
(2) Corma, A.; Iborra, S.; Velty, A. *Chem. Rev.* **2007**, *107*, 2411−2502.
(3) Krenzke, L. D.; Keulks, G. W.; Sklyarov, A. V.; Firsova, A. A.; Kutirev, M. Y.; Margolis, L. Y.; Krylov, O. V. *J. Catal.* **1978**, *52*, 418−424.
(4) Jekewitz, T.; Blickhan, N.; Endres, S.; Drochner, A.; Vogel, H. *Catal. Commun.* **2012**, *20*, 25−28.
(5) Katryniok, B.; Paul, S.; Belliere-Baca, V.; Rey, P.; Dumeignil, F. *Green Chem.* **2010**, *12*, 2079−2098.
(6) Katryniok, B.; Paul, S.; Capron, M.; Dumeignil, F. *ChemSusChem* **2009**, *2*, 719−730.
(7) Ramayya, S.; Brittain, A.; Dealmeida, C.; Mok, W.; Antal, M. J. *Fuel* **1987**, *66*, 1364−1371.
(8) Watanabe, M.; Lida, T.; Aizawa, Y.; Aida, T. M.; Inomata, H. *Bioresour. Technol.* **2007**, *98*, 1285−1290.
(9) Chai, S. H.; Wang, H. P.; Liang, Y.; Xu, B. Q. *J. Catal.* **2007**, *250*, 342−349.
(10) Chai, S. H.; Wang, H. P.; Liang, Y.; Xu, B. Q. *Green Chem.* **2007**, *9*, 1130−1136.
(11) Corma, A.; Huber, G. W.; Sauvanauda, L.; O'Connor, P. *J. Catal.* **2008**, *257*, 163−171.
(12) Tsukuda, E.; Sato, S.; Takahashi, R.; Sodesawa, T. *Catal. Commun.* **2007**, *8*, 1349−1353.
(13) Alhanash, A.; Kozhevnikova, E. F.; Kozhevnikov, I. V. *Appl. Catal., A* **2010**, *378*, 11−18.
(14) Suprun, W.; Lutecki, M.; Haber, T.; Papp, H. *J. Mol. Catal. A: Chem.* **2009**, *309*, 71−78.
(15) Suprun, W.; Lutecki, M.; Papp, H. *Chem. Eng. Technol.* **2011**, *34*, 134−139.
(16) Shiju, N. R.; Brown, D. R.; Wilson, K.; Rothenberg, G. *Top. Catal.* **2010**, *53*, 1217−1223.
(17) Nair, G. S.; Adrijanto, E.; Alsalme, A.; Kozhevnikov, I. V.; Cooke, D. J.; Brown, D. R.; Shiju, N. R. *Catal. Sci. Technol.* **2012**, *2*, 1173−1179.
(18) Katryniok, B.; Paul, S.; Dumeignil, F. *ACS Catal.* **2013**, *3*, 1819−1834.
(19) Nimlos, M. R.; Blanksby, S. J.; Qian, X. H.; Himmel, M. E.; Johnson, D. K. *J. Phys. Chem. A* **2006**, *110*, 6145−6156.
(20) Laino, T.; Tuma, C.; Curioni, A.; Jochnowitz, E.; Stolz, S. *J. Phys. Chem. A* **2011**, *115*, 3592−3595.
(21) Yoda, E.; Ootawa, A. *Appl. Catal., A* **2009**, *360*, 66−70.
(22) Kim, Y. T.; Jung, K. D.; Park, E. D. *Appl. Catal., B* **2011**, *107*, 177−187.
(23) Copeland, J. R.; Shi, X.-R.; Sholl, D. S.; Sievers, C. *Langmuir* **2013**, *29*, 581−593.
(24) Copeland, J. R.; Santillan, I. A.; Schimming, S. M.; Ewbank, J. L.; Sievers, C. *J. Phys. Chem. C* **2013**, *117*, 21413−21425.
(25) Nowak, I.; Ziolek, M. *Chem. Rev.* **1999**, *99*, 3603−3624.
(26) Datka, J.; Turek, A. M.; Jehng, J. M.; Wachs, I. E. *J. Catal.* **1992**, *135*, 186−199.
(27) Chen, Z.; Iizuka, T.; Tanabe, K. *Chem. Lett.* **1984**, 1085−1088.
(28) Tanabe, K.; Okazaki, S. *Appl. Catal., A* **1995**, *133*, 191−218.
(29) Nakajima, K.; Baba, Y.; Noma, R.; Kitano, M.; Kondo, J. N.; Hayashi, S.; Hara, M. *J. Am. Chem. Soc.* **2011**, *133*, 4224−4227.
(30) Brunauer, S.; Emmett, P. H.; Teller, E. *J. Am. Chem. Soc.* **1938**, *60*, 309−319.
(31) Barrett, E. P.; Joyner, L. G.; Halenda, P. P. *J. Am. Chem. Soc.* **1951**, *73*, 373−380.
(32) Kresse, G.; Hafner, J. *Phys. Rev. B* **1993**, *47*, 558−561.
(33) Kresse, G.; Hafner, J. *Phys. Rev. B* **1994**, *49*, 14251−14269.
(34) Kresse, G.; Furthmuller, J. *Comput. Mater. Sci.* **1996**, *6*, 15−50.
(35) Kresse, G.; Furthmuller, J. *Phys. Rev. B* **1996**, *54*, 11169−11186.
(36) Perdew, J. P.; Chevary, J. A.; Vosko, S. H.; Jackson, K. A.; Pederson, M. R.; Singh, D. J.; Fiolhais, C. *Phys. Rev. B* **1992**, *46*, 6671−6687.
(37) Perdew, J. P.; Chevary, J. A.; Vosko, S. H.; Jackson, K. A.; Pederson, M. R.; Singh, D. J.; Fiolhais, C. *Phys. Rev. B* **1993**, *48*, 4978−4978.
(38) Blochl, P. E. *Phys. Rev. B* **1994**, *50*, 17953−17979.
(39) Kresse, G.; Joubert, D. *Phys. Rev. B* **1999**, *59*, 1758−1775.
(40) Kato, K.; Tamura, S. *Acta Crystallogr., Sect. B: Struct. Sci.* **1975**, *31*, 673−677.
(41) Bergerhoff, G.; Brown, I. D. *Crystallographic Databases*; International Union of Crystallography: Chester, U. K., 1987.
(42) Sholl, D.; Steckel, J. A. *Density Functional Theory: A Practical Introduction*; John Wiley & Sons: Hoboken, NJ, 2009; p 114.
(43) Iizuka, T.; Ogasawara, K.; Tanabe, K. *Bull. Chem. Soc. Jpn.* **1983**, *56*, 2927−2931.
(44) Jehng, J. M.; Wachs, I. E. *J. Phys. Chem.* **1991**, *95*, 7373−7379.
(45) Burcham, L. J.; Datka, J.; Wachs, I. E. *J. Phys. Chem. B* **1999**, *103*, 6015−6024.
(46) Pittman, R. M.; Bell, A. T. *J. Phys. Chem.* **1993**, *97*, 12178−12185.
(47) Gott, T.; Oyama, S. T. *J. Catal.* **2009**, *263*, 359−371.
(48) Popova, G. Y.; Chesalov, Y. A.; Sadovskaya, E. M.; Andrushkevich, T. V. *J. Mol. Catal. A: Chem.* **2012**, *357*, 148−153.
(49) Clayden, J.; Greeves, N.; Warren, S. *Organic Chemistry*, 2nd ed.; Oxford University Press: New York, 2012; p 498.
(50) Delgado, M.; Desroches, M.; Ganachaud, F. *RSC Adv.* **2013**, *3*, 23057−23065.
(51) Yaylayan, V. A.; Harty-Majors, S.; Ismail, A. A. *J. Agric. Food Chem.* **1999**, *47*, 2335−40.
(52) de Jesus, J. C.; Zaera, F. *Surf. Sci.* **1999**, *430*, 99−115.
(53) Copeland, J. R.; Foo, G. S.; Harrison, L. A.; Sievers, C. *Catal. Today* **2013**, *205*, 49−59.
(54) Raman, M. S.; Ponnuswamy, V.; Kolandaivel, P.; Perumal, K. *J. Mol. Liq.* **2008**, *142*, 10−16.
(55) Socrates, G. *Infrared and Raman Characteristic Group Frequencies*, 3rd ed.; John Wiley & Sons Ltd: England, 2001; p 122.
(56) Palumbo, L.; Bonino, F.; Beato, P.; Bjorgen, M.; Zecchina, A.; Bordiga, S. *J. Phys. Chem. C* **2008**, *112*, 9710−9716.
(57) Karge, H. G.; Niessen, W.; Bludau, H. *Appl. Catal., A* **1996**, *146*, 339−349.
(58) Rozwadowski, M.; Lezanska, M.; Wloch, J.; Erdmann, K.; Golembiewski, R.; Kornatowski, J. *Chem. Mater.* **2001**, *13*, 1609−1616.
(59) Colthup, N. B.; Daly, L. H.; Wiberley, S. E. *Introduction to Infrared and Raman Spectroscopy*, 3rd ed.; Academic Press: Waltham, MA, 1990; p 261.
(60) Popov, A.; Kondratieva, E.; Goupil, J. M.; Mariey, L.; Bazin, P.; Gilson, J. P.; Travert, A.; Mauge, F. *J. Phys. Chem. C* **2010**, *114*, 15661−15670.
(61) Pinard, L.; Tayeb, K. B.; Hamieh, S.; Vezin, H.; Canaff, C.; Maury, S.; Delpoux, O.; Pouilloux, Y. *Catal. Today* **2013**, *218−219*, 57−64.
(62) Broclawik, E.; Kozyra, P.; Datka, J. *C. R. Chim.* **2005**, *8*, 491−508.
(63) Hall, R. H.; Stern, E. S. *J. Chem. Soc.* **1950**, 490−498.
(64) Luthi-Peng, Q.; Scharer, S.; Puhan, Z. *Appl. Microbiol. Biotechnol.* **2002**, *60*, 73−80.
(65) Vollenweider, S.; Grassi, G.; Konig, I.; Puhan, Z. *J. Agric. Food Chem.* **2003**, *51*, 3287−3293.
(66) Ravenelle, R. M.; Copeland, J. R.; Van Pelt, A. H.; Crittenden, J. C.; Sievers, C. *Top. Catal.* **2012**, *55*, 162−174.
(67) Jongerius, A. L.; Copeland, J. R.; Foo, G. S.; Hofmann, J. P.; Bruijnincx, P. C. A.; Sievers, C.; Weckhuysen, B. M. *ACS Catal.* **2013**, *3*, 464−473.
(68) Tamura, M.; Shimizu, K.-i.; Satsuma, A. *Appl. Catal., A* **2012**, *433*, 135−145.
(69) Kinage, A. K.; Upare, P. P.; Kasinathan, P.; Hwang, Y. K.; Chang, J. S. *Catal. Commun.* **2010**, *11*, 620−623.
(70) Tokmachev, A. M.; Pushkar, Y. N.; Fionov, A. V.; Lunina, E. V.; Chuvylkin, N. D. *Russ Chem. Bull.* **2000**, *49*, 991−996.
(71) Olah, G. A.; Baker, E. B.; Evans, J. C.; Tolgyesi, W. S.; McIntyre, J. S.; Bastien, I. J. *J. Am. Chem. Soc.* **1964**, *86*, 1360−1373.

(72) ten Dam, J.; Hanefeld, U. *ChemSusChem* **2011**, *4*, 1017−1034.
(73) Wang, Z.; Wang, L.; Jiang, Y.; Hunger, M.; Huang, J. *ACS Catal.* **2014**, *4*, 1144−1147.
(74) Galhotra, P.; Navea, J. G.; Larsen, S. C.; Grassian, V. H. *Energy Environ. Sci.* **2009**, *2*, 401−409.
(75) Garcia-Sancho, C.; Moreno-Tost, R.; Merida-Robles, J.; Santamaria-Gonzalez, J.; Jimenez-Lopez, A.; Maireles-Torres, P. *Appl. Catal., A* **2012**, *433*, 179−187.
(76) Wang, F.; Dubois, J. L.; Ueda, W. *J. Catal.* **2009**, *268*, 260−267.
(77) Wang, F.; Dubois, J. L.; Ueda, W. *Appl. Catal., A* **2010**, *376*, 25−32.
(78) Gu, Y. L.; Cui, N. Y.; Yu, Q. J.; Li, C. Y.; Cui, Q. K. *Appl. Catal., A* **2012**, *429*, 9−16.
(79) Possato, L. G.; Diniz, R. N.; Garetto, T.; Pulcinelli, S. H.; Santilli, C. V.; Martins, L. *J. Catal.* **2013**, *300*, 102−112.
(80) Bartholomew, C. H. *Appl. Catal., A* **2001**, *212*, 17−60.